Elastic scattering, inelastic excitation, and 1*n* pick-up transfer cross sections for ^{10}B + ^{120}Sn at energies near the Coulomb barrier

M. A. G. Alvarez* and M. Rodríguez-Gallardo
Departamento FAMN, Universidad de Sevilla, Apartado 1065, 41080 Sevilla, Spain

L. R. Gasques, L. C. Chamon, J. R. B. Oliveira, V. Scarduelli, A. S. Freitas, and E. S. Rossi, Jr.
Instituto de Física da Universidade de São Paulo, 05508-090, São Paulo, SP, Brazil

V. A. B. Zagatto, J. Rangel, and J. Lubian
Instituto de Física da Universidade Federal Fluminense, 24210-346, Niterói, Rio de Janeiro, Brazil

I. Padron
Centro de Aplicaciones Tecnológicas y Desarrollo Nuclear, 502, Calle 30, La Habana, Cuba

(Received 21 June 2018; published 24 August 2018)

The ^{10}B + ^{120}Sn reaction has been systematically studied at laboratory energies around the Coulomb barrier: $E_{\rm LAB}$ = 31.5, 33.5, 35.0, and 37.5 MeV. Cross sections for the elastic scattering and some reaction processes have been measured: excitation to the 1^+ state of ^{10}B; excitation to the 2^+ and 3^- states of ^{120}Sn; and the one-neutron pick-up transfer ^{120}Sn(^{10}B,^{11}B)^{119}Sn. Coupled reaction channel (CRC) calculations have been performed in the context of the double-folding São Paulo potential. The theoretical calculations result in a good overall description of the experimental angular distributions. The effect on the theoretical elastic-scattering angular distributions of couplings to the inelastic and transfer states (through the CRC calculations) and to the continuum states (through continuum-discretized coupled-channels calculations) has been investigated.

DOI: 10.1103/PhysRevC.98.024621

I. INTRODUCTION

Exotic and weakly bound nuclei originated in the primordial nucleosynthesis. In particular, the exotic ^{7}Be and the stable weakly bound ^{7}Li were formed with very small yields. Nuclei heavier than ^{7}Be and ^{7}Li have been formed much later in the stellar nucleosynthesis, through light nuclei (H, He, Li, Be, B, etc.) reacting during star evolution or explosion. Thus, the interstellar medium contains declining abundances of the light nuclei. On the other hand, the yields of light nuclei in the universe are also influenced by cosmic-ray (mainly high-energy protons) spallation. This process is responsible for breaking the heavy elements up in the interstellar medium. In such a scenario, any model to explain the current abundances of light nuclei must connect the stellar nucleosynthesis with the primordial one [1].

The study of exotic and stable weakly bound nuclei is one of the forefronts of current research in nuclear physics [2]. Recently developed facilities, worldwide, that produce radioactive ion beams provide opportunities to probe new aspects of nuclear physics [3–5] and astrophysics [6]. The discovery of halo nuclei revealed that some exotic nuclei could have an extraordinary size [7]. This discovery triggered many experimental and theoretical works to search for nuclei with unusual properties, such as an anomalous large radius or enhanced breakup cross sections. Nowadays, several nuclei, such as ^{6}He, ^{11}Li, and ^{11}Be, are well known to present a halo structure, where a core is surrounded by one or two weakly bound nucleons, giving rise to a diffuse matter distribution that can produce an enhanced breakup cross section, even well below the Coulomb barrier [8–16]. In addition, reactions of exotic and stable weakly bound nuclei at energies around the Coulomb barrier revealed the importance of the corresponding structure in the dynamics of the reaction processes, since it provides insight into degrees of freedom connected to slow processes.

Studying reactions involving weakly bound stable nuclei is a crucial step towards a better understanding of the exotic ones. Comparing them is important for systematic studies with the purpose of determining how these nuclei react, aiming also to understand their respective abundances. Exotic and stable weakly bound nuclei have two common fundamental characteristics: low breakup threshold and cluster structure. The breakup when interacting with another nucleus gives rise to a complex problem of three or more bodies. Breakup can occur by direct excitation to the weakly bound projectile into continuum states, or by populating continuum states of the target [9–12,17–19]. Close to or even below the Coulomb barrier, the Coulomb breakup even dominates some reactions of exotic nuclei with heavy targets [20]. In nuclear astrophysics, Coulomb breakup of weakly bound projectiles has been used as an indirect method for determining cross sections of radioactive capture processes [21–23].

*malvarez@us.es

 ©2018 American Physical Society

Weakly bound stable nuclei can easily be produced and accelerated in conventional particle accelerators, where the reactions with several targets allow systematic studies with high statistics. Within this context, the E-125 experimental campaign has been developed at the Open Laboratory of Nuclear Physics (LAFN, acronym in Portuguese) at the Institute of Physics of the University of São Paulo (IFUSP, acronym in Portuguese). The aim of the project is to study the scattering involving the light weakly bound stable nuclei ^{6}Li, ^{7}Li, ^{9}Be, ^{10}B, and ^{11}B, on the same heavy target (^{120}Sn), at energies around the Coulomb barriers, and compare the respective results among them as well as with others reactions involving exotic nuclei ^{6,8}He, ^{8,9,11}Li, ^{10,11}Be. These reactions with the ^{120}Sn target have produced many channels of inelastic excitation and transfer, which can be conveniently separated in the experimental energy spectra [24,25]. The analyses of the different nuclear reactions processes, at several energies and within the same theoretical approach, represent a powerful breakthrough.

For ^{7}Li + ^{120}Sn, we measured the elastic scattering, the excitation to the $1/2^{-}$ ^{7}Li first-excited state ($E^{*} = 478$ keV), the excitation to the 2^{+} and 3^{-} ^{120}Sn states ($E^{*} = 1171$ and 2400 keV), and the one-neutron stripping reaction, at energies close to the barrier [V_B(LAB) $\approx$ 20.6 MeV]: $E_{\rm LAB} = 20$, 22, 24, and 26 MeV [24]. For this system, coupled reaction channel (CRC) calculations have been performed in the context of the double-folding São Paulo potential (SPP) [26,27]. It turns out that the inclusion of the $1/2^{-}$ ^{7}Li first-excited state as well as the projectile coupling to the continuum (α plus a tritium particle) play a fundamental role in the simultaneous description of the elastic, inelastic, and transfer cross sections. In particular, the simulation of the breakup effect, through the trivial local equivalent potential, suggests the importance of couplings to the continuum. On the contrary, the coupling to the one-neutron stripping channel does not significantly affect the theoretical elastic- and inelastic-scattering angular distributions.

Similar to ^{7}Li, ^{10}B also presents a first-excited state with low excitation energy (1^{+}, 718 keV). Furthermore, it is a weakly bound stable nucleus that may break up into different mass partitions, being the most energetically favorable the $^{10}\mathrm{B} \rightarrow {}^{6}\mathrm{Li} + {}^{4}\mathrm{He}$ ($Q = -4.461$ MeV). In such a scenario, it could be important to include couplings to continuum states in order to describe simultaneously the elastic scattering and the different reaction channels. As part of the E-125 experimental campaign, the ^{10}B + ^{120}Sn reaction has already been measured at 37.5 MeV and analyzed within the CRC formalism [25]. In the present work, we report on new experimental results obtained for the same reaction measured at $E_{\rm LAB} = 31.5, 33.5$, and 35.0 MeV. Here, we present theoretical results obtained through CRC calculations and also those within the context of the continuum-discretized coupled channels (CDCCs).

In the next section, the experimental setup presented in Refs. [24,25] is revisited. Then, we present the experimental data and respective theoretical analyses. Finally, we discuss our results and present the main conclusions.

II. EXPERIMENTAL SETUP

The development of new instrumentation has allowed more complex nuclear reaction measurements at the LAFN. The results of such experiments seek to answer some of the relevant questions regarding the understanding of cluster-like properties of light nuclei and how these properties influence reactions.

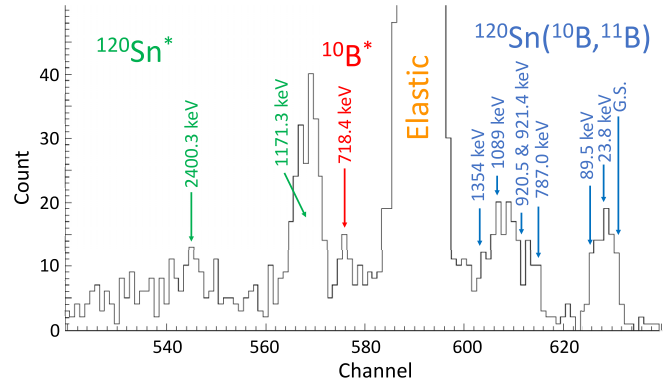

FIG. 1. Spectrum taken at $\theta_{\rm LAB} = 125^{\circ}$ and $E_{\rm LAB} = 35$ MeV. The peaks corresponding to the $1n$ pick-up transfer (blue), elastic scattering of ^{10}B on ^{120}Sn (orange), inelastic excitation to the 1^{+} ^{10}B first-excited state (red), and the excitation to the 2^{+} and 3^{-} ^{120}Sn states (green), can be clearly identified in the figure.

As previously mentioned, the experiment ^{10}B + ^{120}Sn is part of the E-125 campaign that has been carried out at the LAFN. The experimental setup is based on SATURN (Silicon Array based on Telescopes of USP for Reactions and Nuclear applications). SATURN is being developed as a portable nuclear reaction spectrometer, based on silicon-detector telescopes, desktop-type electronic modules, and multichannel acquisition systems. SATURN is installed in the 30B experimental beam line of the laboratory, which contains a scattering chamber connected to the 8 MV pelletron tandem accelerator [24,25].

The reaction ^{10}B + ^{120}Sn was measured at the bombarding energies $E_{\rm lab} = 31.5$, 33.5, 35.0, and 37.5 MeV. The SATURN detecting system was mounted with nine surface barrier detectors in angular intervals of 5°, covering 40° in each run. Normally, with 3 runs we cover approximately 120°, from 40° to 160°. The energy calibration of each detector was performed following the same procedure adopted in Ref. [25].

As illustration, a typical spectrum taken at $E_{\rm LAB} = 35$ MeV and $\theta_{\rm LAB} = 125^{\circ}$ is shown in Fig. 1. All the peaks have been identified and labeled by using different colors. The elastic-scattering peak of ^{10}B incident on ^{120}Sn is labeled in orange. The peak relative to the 1^{+} ^{10}B inelastic excitation is given in red, while the excitation to the 2^{+} and 3^{-} ^{120}Sn states are indicated by the green arrows. The peaks corresponding to different energy levels of the $1n$ pick-up transfer are indicated by the blue arrows. For this reaction, different states of the compound ^{119}Sn nucleus are separated and integrated in two groups. These groups can be identified in the spectrum of Fig. 1: the first group refers to the ground-state (g.s.), 23.8, and 89.5 keV excited states, and the second group refers to the 787.0, 920.5, 921.4, 1089, and 1354 keV excited states.

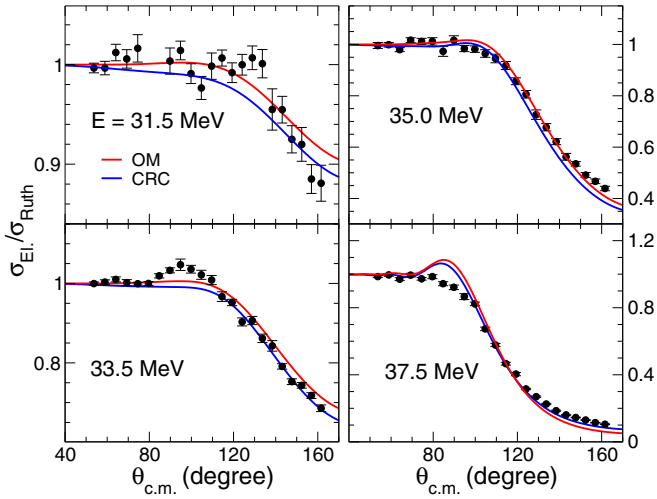

FIG. 2. Experimental and theoretical results for the elastic-scattering angular distributions of ^{10}B + ^{120}Sn at different bombarding energies.

III. EXPERIMENTAL DATA AND COUPLED REACTION CHANNEL CALCULATIONS

In this section, we present an analysis of the elastic scattering and reaction channels. With this aim, we have performed CRC calculations as well as (elastic-scattering) single-channel optical model (OM) calculations. The SPP is assumed for the real part of the optical potential. For the imaginary part, we have assumed the SPP multiplied by a fixed normalization factor, $N_I = 0.25$, that has provided the best results in the previous CRC data analyses for $E_{\rm LAB} = 37.5$ MeV [25]. The FRESCO code was used to calculate the theoretical cross sections. As in Ref. [25], the collective vibrational mode was assumed to describe the quadrupole and octupole excited states of the ^{120}Sn, whereas the ^{10}B was treated as a rotor. All the parameter values assumed in the present CRC calculations (which are provided in Tables I–III of Ref. [25]) have been determined in the previous data analyses for $E_{\rm LAB} = 37.5$ MeV. In this sense, no adjustable parameters are involved in the description of the data for the other energies. Thus, for $E_{\rm LAB} = 31.5$, 33.5, and 35.0 MeV we, in fact, deal with theoretical predictions instead of data fits.

A. Elastic scattering

Figure 2 presents experimental data and theoretical calculations for the elastic-scattering angular distributions at the bombarding energies of 31.5, 33.5, 35.0, and 37.5 MeV. The red and blue lines in the figure refer to OM and CRC calculations, respectively. Since both kinds of calculations were performed with the same optical potential, the difference between the curves directly translates the effect of the couplings.

The effect of the couplings is not very significant. Both calculations (CRC and OM) reproduce reasonably the data for all energies. Unlike other energies, the experimental data at 33.5 MeV present a Fresnel peak around 100°, which is not reproduced by the theoretical calculations. On the other hand, the pronounced Fresnel peak that is present in the theoretical angular distributions at 37.5 MeV is absent from the data. Thus, the CRC calculations do not reproduce the data taken at 33.5 and 37.5 MeV around the Fresnel angular region. Because ^{10}B can be considered a cluster formed by ^{4}He + ^{6}Li, it is important to test the effect of the couplings to continuum states. This is the subject of Sec. IV.

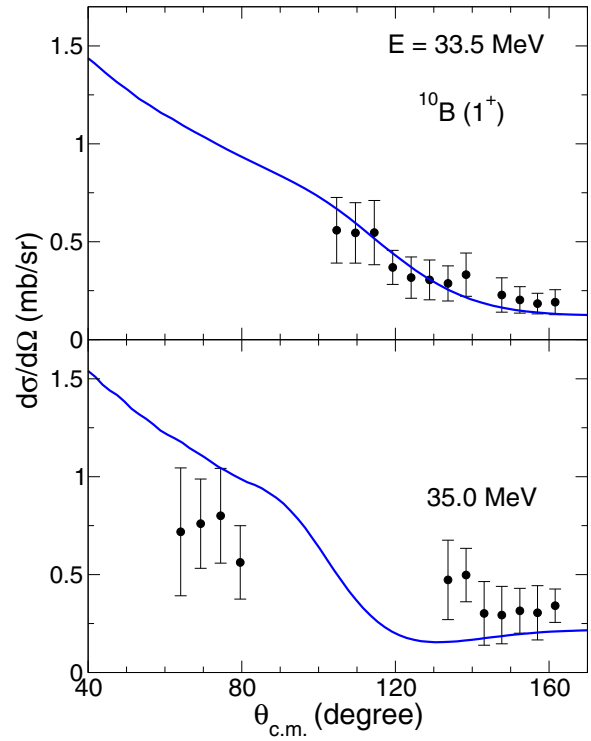

FIG. 3. Inelastic-scattering angular distributions for the quadrupole excitation in ^{10}B.

B. Inelastic excitation

Figure 3 presents the cross sections for the inelastic excitation of the 1^+ state of ^{10}B ($E^* = 0.718$ MeV) at 33.5 and 35.0 MeV, while Fig. 4 shows the angular distributions for the excitation to the 2^+ ^{120}Sn state ($E^* = 1.171$ MeV) at 31.5, 33.5, and 35.0 MeV. The results of the CRC calculations are in good agreement with the data for all these cases. Figure 5 presents the angular distributions for the inelastic excitation to the 3^- ^{120}Sn state ($E^* = 2.400$ MeV) at 33.5 and 35.0 MeV. Again, data and CRC theoretical calculations are compatible within the error bars. However, as already discussed in Ref. [25], we point out that the data for inelastic excitation may have some contamination (in the experimental spectra) related to the $1n$ transfer process populating high excited states of ^{119}Sn.

C. One-neutron-transfer cross sections

Experimental differential cross sections for $1n$ pick-up, ^{120}Sn(^{10}B, ^{11}B)^{119}Sn ($Q_{\rm g.s.} = 2.350$ MeV), have been obtained for different states of the residual ^{119}Sn nucleus. As reported in Ref. [25] for 37.5 MeV, the yields corresponding to different states of ^{119}Sn could not be determined individually. In fact, two relatively broad peaks were observed in the spectra

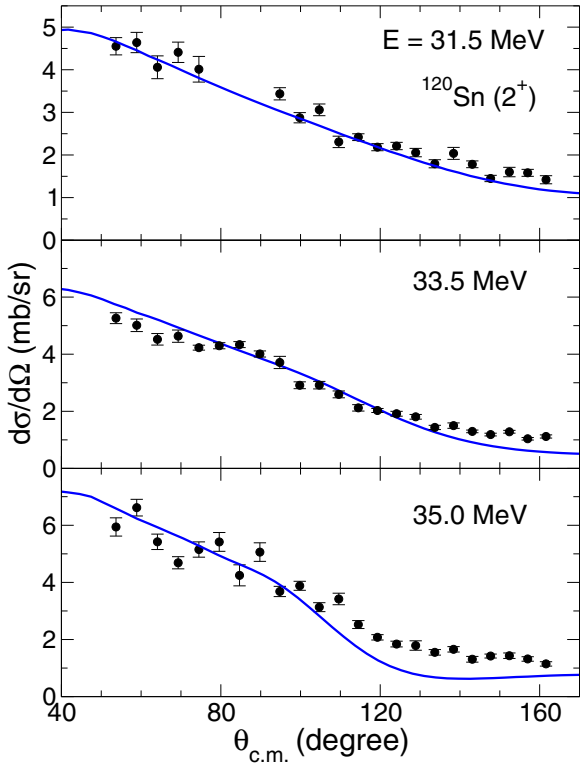

FIG. 4. Inelastic-scattering angular distributions for the quadrupole excitation in ^{120}Sn.

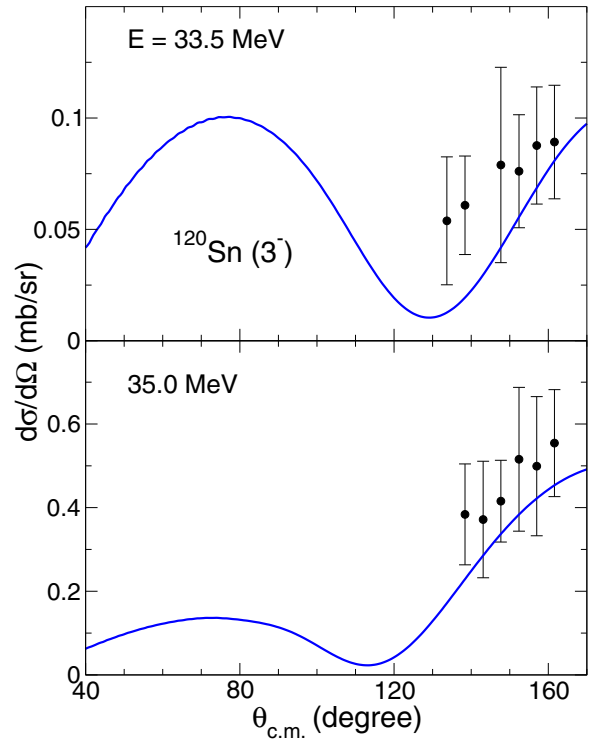

FIG. 5. Inelastic-scattering angular distributions for the octupole excitation in ^{120}Sn.

(see Fig. 1). The first group includes the g.s., 23.8, and 89.5 keV states, whereas the second group includes the 787.0, 920.5, 921.4, 1089, and 1354 keV states.

Before presenting the analyses for the other energies, we comment on the main results obtained (in Ref. [25]) from the data analyses for $E_{\rm LAB} = 37.5$ MeV. The Woods–Saxon shape was assumed for the nuclear potentials of the neutron-core systems ($n + {}^{10}$B and $n + {}^{119}$Sn). The corresponding values for the radius, diffuseness, and depth for the g.s. of ^{11}B and ^{120}Sn are listed in Table II of Ref. [25]. The depth for each state is automatically adjusted by the FRESCO code in order to reproduce the corresponding biding energies. The inclusion of spin-orbit potentials for the $n + {}^{10}$B and $n + {}^{119}$Sn systems has a negligible effect on the calculated transfer angular distributions. The spectroscopic factor values assumed for states of the overlap $\langle {}^{120}\text{Sn}|{}^{119}\text{Sn} + n\rangle$ are given in Table III of Ref. [25]. For the overlap $\langle {}^{10}\text{B}|{}^{9}\text{B} + n\rangle$, we have obtained several different sets of values for the spectroscopic factor and potential parameters that provide quite similar theoretical angular distributions for the neutron transfer process. This ambiguity is extensively discussed in Ref. [25].

In the present work, we have performed CRC calculations for all energies in the same conditions as reported in Ref. [25]. The ambiguity observed in 37.5 MeV (commented in the previous paragraph) is also observed for the other energies. Figures 6–8 present experimental and theoretical (CRC) 1n pick-up transfer cross sections measured at 31.5, 33.5, and 35.0 MeV. The cross sections correspond to the sum of the individual contributions relative to different excited states of ^{119}Sn. Considering the lack of adjustable parameters, the agreement between data and theoretical results is remarkable for all energies.

IV. EFFECT OF BREAKUP CHANNELS ON ELASTIC SCATTERING

As described in the last section, the CRC calculations provide a quite reasonable simultaneous description of the data relative to the elastic scattering, projectile and target excitations, and neutron transfer processes. The only significant

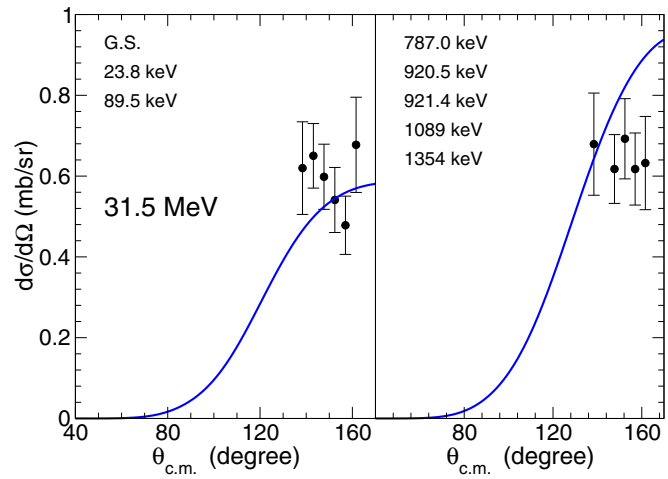

FIG. 6. 1n pick-up transfer angular distributions at 31.5 MeV.

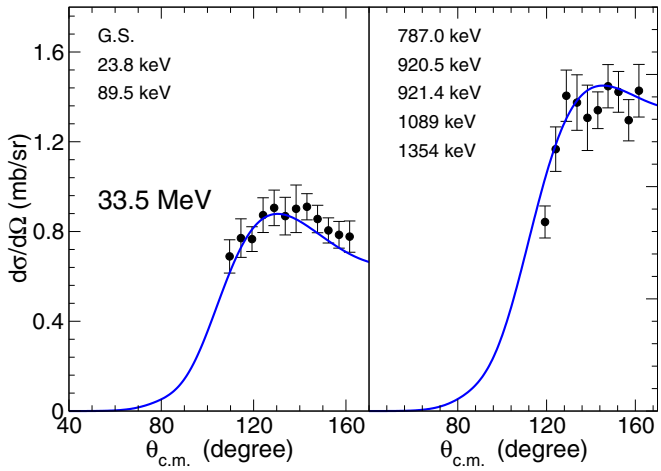

FIG. 7. Same as Fig. 6 but for 33.5 MeV.

disagreement between theory and experiment is observed for the elastic scattering at the Fresnel angular region. Thus, we performed CDCC calculations in order to verify whether that discrepancy would be related to the couplings to the continuum states.

The binding energy of ^{10}B is 4.461 MeV when it breaks into an alpha particle plus a ^{6}Li nucleus. Despite having a low breakup threshold of 1.473 MeV, the sequential breakup of the ^{6}Li fragment is not considered in our calculations since it is a second-order interaction. To account for the effect of the breakup channel on the elastic-scattering angular distributions, we have assumed the standard CDCC method [28–30], using the cluster model to describe the states of the projectile. This means that, in our CDCC calculations, we have not included the target excitations or the transfer channels. In fact, our CRC calculations demonstrated that such couplings do not have significant effect on the elastic scattering angular distributions.

To perform CDCC calculations, one expands the total wave function of the system, for the total angular momentum J and projection M, in states of a basis as

$$\Psi^{JM}(\mathbf{R},\mathbf{r}) = \sum_{\alpha} \frac{f_{\alpha,J}(R)}{R} \mathcal{Y}_{\alpha}^{JM}(\hat{\mathbf{R}},\mathbf{r}), \tag{1}$$

where $\mathbf{r}$ represents the internal intrinsic coordinate of the projectile and $\mathbf{R}$ is the projectile-target relative coordinate. In Eq. (1), $\mathcal{Y}_{\alpha}^{JM}(\hat{\mathbf{R}},\mathbf{r})$ represents the tensor product of the angular part of the projectile-target relative wave function with the intrinsic wave function of the projectile. In this expansion, we use the binning method to generate the basis of square-integrable wave functions of the projectile. They are obtained by taking the energy average of ^{6}Li+α scattering states within a given energy range (bin). They are then labeled by the midpoint of the energy interval and by its angular momentum. We consider orbital angular momenta up to $l = 3\hbar$. Using these states, the g.s. and the bound-states with energy lower than the binding energy of the clusters, one builds an orthonormal basis to describe the continuum space of the projectile. The details of this procedure can be found in Refs. [31,32].

Inserting Eq. (1) into the Schrödinger equation and carrying out some algebra, one obtains the following set of coupled equations:

$$[H_{\alpha} - (E-\varepsilon_{\alpha})] f_{\alpha,J}(R) + \sum_{\alpha' \neq \alpha} i^{L'-L} V_{\alpha\alpha'}(R) f_{\alpha',J}(R) = 0, \tag{2}$$

where

$$H_{\alpha} = -\frac{\hbar^2}{2\mu}\left[\frac{d^2}{dR^2} - \frac{L(L+1)}{R^2}\right] + V_{\alpha\alpha}(R) \tag{3}$$

is the Hamiltonian in channel α, and ε_{α} is the intrinsic energy of the projectile in this channel. In the present calculation, $\alpha = 0$ stands for the elastic channel, where the projectile is in its g.s. ($\varepsilon_0 = 0,\ l_0 = 2,\ j_0 = 3$), and $\alpha \neq 0$ corresponds to a projectile's state of an excited bound state or of a continuum bin state, with energy ε_{α}.

The matrix elements of Eq. (2) are given by

$$V_{\alpha\alpha'}(R) = \langle \phi_{\alpha}(\mathbf{r}) | V(\mathbf{R},\mathbf{r}) | \phi_{\alpha'}(\mathbf{r}) \rangle, \tag{4}$$

where $\phi_{\alpha}(\mathbf{r})$ stands for the wave functions of both bound states and bins of the projectile.

The projectile-target interaction is given by the sum

$$V(\mathbf{R},\mathbf{r}) = V_{^{4}\mathrm{He}-^{120}\mathrm{Sn}}(\mathbf{r}_{\mathrm{v}}) + V_{^{6}\mathrm{Li}-^{120}\mathrm{Sn}}(\mathbf{r}_{\mathrm{c}}), \tag{5}$$

where $V_{^{4}\mathrm{He}-^{120}\mathrm{Sn}}$ and $V_{^{6}\mathrm{Li}-^{120}\mathrm{Sn}}$ are the optical potentials responsible for the elastic scattering of the valence particle (^{4}He) and of the core (^{6}Li) on the target (^{120}Sn). They are functions of the position vectors of the valence particle ($\mathbf{r}_{\mathrm{v}}$) and the core ($\mathbf{r}_{\mathrm{c}}$), respectively. These vectors are given in terms of the vector joining the centers of the collision partners ($\mathbf{R}$) and the vector between the valence particle and the core ($\mathbf{r}$), by the standard relations

$$\mathbf{r}_{\mathrm{v}} = \mathbf{R} + \frac{A_{\mathrm{c}}}{A_p}\mathbf{r} \text{ and } \mathbf{r}_{\mathrm{c}} = \mathbf{R} - \frac{A_{\mathrm{v}}}{A_p}\mathbf{r}, \tag{6}$$

where A_{c}, A_{v}, and A_p are the mass numbers of the core, the valence particle, and the projectile, respectively.

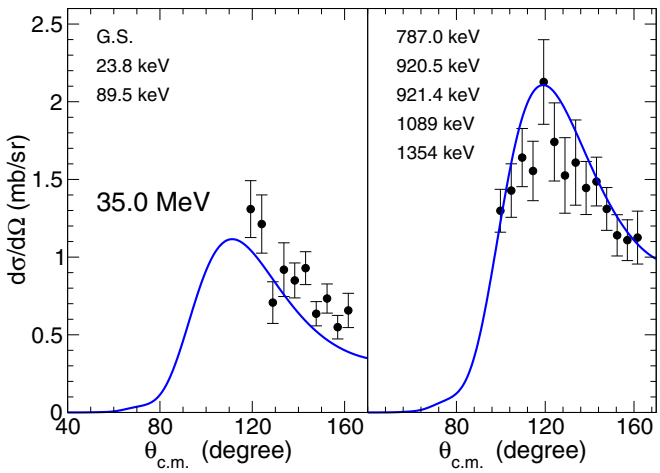

FIG. 8. Same as Fig. 6 but for 35.0 MeV.

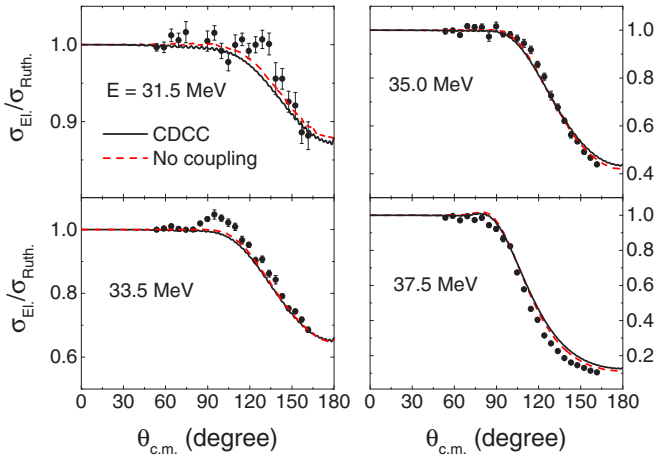

FIG. 9. Experimental and CDCC results for the elastic-scattering angular distributions. The no-coupling case corresponds to the results of the CDCC calculations turning off the couplings.

The SPP was assumed for the real and imaginary parts of the $V_{^4\mathrm{He}-^{120}\mathrm{Sn}}$ and $V_{^6\mathrm{Li}-^{120}\mathrm{Sn}}$ optical potentials. The strength coefficient of the imaginary part was set as $N_I = 0.78$. This strength coefficient has shown to be able to describe the elastic scattering of many systems involving tightly bound nuclei, in wide mass and energy ranges [27]. All intrinsic states of the projectile (bound and unbound) were determined by solving the Schrödinger equation for the ^{6}Li+α system, assuming the SPP for the real part of the potential.

For the four energies studied in this work, the convergence of the CDCC method was checked in detail to warrant that the results do not depend on the model space used. To solve the set of coupled equations [Eq. (2)], the matrix elements $V_{\alpha\alpha'}(R)$ are expanded in multipoles up to $\lambda = 3$, and their multipole components are evaluated by numerical integration over a mesh of radial distances (between the core and the valence particle) distributed between $r = 0$ and $r_{\max} = 80$ fm, with integration step size of 0.02 fm. The coupled equations are then solved numerically considering projectile-target distances up to $R =$ 1000 fm and angular momenta up to $500\hbar$. The maximum bin energy for all the energies was 10 MeV. The width of the bins were 2.0 MeV for the two lower bombarding energies, while it was 1.5 MeV for the other two energies.

Data and theoretical results for the elastic-scattering angular distributions, at the four bombarding energies, are presented in Fig. 9. The solid black lines in these figures correspond to the cross sections obtained with the CDCC calculations considering the couplings to the bound and continuum states, while the dashed red lines (labeled by no coupling) represent the CDCC results obtained turning off the couplings (remaining, therefore, only the g.s.). We point out that the no coupling calculations account for the cluster structure of the projectile in the g.s., i.e., the optical potential of this case corresponds to that given in expressions (4) and (5), with $\alpha = 0$.

The no-coupling theoretical cross sections presented in Fig. 9 are rather different from those of the OM in Fig. 2. In particular, the (theoretical) Fresnel peak at 37.5 MeV shown in Fig. 9 is much less pronounced than that in Fig. 2. Both sets of theoretical cross sections are obtained from single-channel (g.s.) calculations but with different optical potentials. In fact, the results presented in Fig. 9 were obtained through Eqs. (4) and (5), while those of Fig. 2 derive from the SPP. Of course, these two potentials should not be identical.

The results presented in Fig. 9 indicate that the effect of the couplings on the continuum on the elastic-scattering cross sections is very small. In particular, the discrepancy observed in Fig. 2 between theory and experiment at 33.5 MeV in the Fresnel angular region is still present in the results shown in Fig. 9 for the CDCC calculations. We mention that ^{10}B can also be broken into $p + {}^9$Be and $d + {}^8$Be, with breakup thresholds larger than 6 MeV. Because the binding energy is higher, one should expect that these two breakup modes should affect the elastic-scattering distribution less than the breakup mode studied here.

Therefore, our theoretical calculations do not explain the behavior of the elastic-scattering angular distributions at the Fresnel region. On the other hand, we have confidence that no significant systematic errors are present in the data set. In fact, the measurements for all energies, including 37.5 MeV, were performed in two consecutive weeks, using the same experimental setup and target. The setup consisted of a dedicated nuclear reaction chamber, vacuum, mechanics, electronics, and data-acquisition system, already used to perform measurements for other systems, such as, for instance, ^{7}Li + ^{120}Sn [24]. As reported in Ref. [25], we have used thin ($\approx$100 μg/cm^2) isotopically enriched (>99%) ^{120}Sn targets, with a thin backing layer of ^{197}Au for normalization purposes (at this energy range, the corresponding elastic-scattering cross section is associated with the Rutherford one). With this, the cross sections can be accurately obtained, since they are related to the ratio between yields of ^{120}Sn and ^{197}Au. No trace of any kind of contaminants has been observed during the whole experimental campaign.

V. SUMMARY AND CONCLUSION

As part of the E-125 experimental campaign that has been carried out at the LAFN, measurements for the ^{10}B + ^{120}Sn system have been performed at the bombarding energies of 31.5, 33.5, 35.0, and 37.5 MeV. Besides the elastic-scattering channel, the excitation to the 1^+ state of ^{10}B, the excitation to the 2^+ and 3^- states of ^{120}Sn, and the one-neutron pick-up transfer reaction ^{120}Sn(^{10}B, ^{11}B)^{119}Sn have been observed. The results corresponding to the measurement taken at 37.5 MeV were previously published in Ref. [25]. A simultaneous analysis of the cross sections of these different channels has been performed within the CRC and OM formalisms in the context of the double-folding SPP interaction. The imaginary part of the optical potential that provides the best data fit for $E_{\mathrm{LAB}} = 37.5$ MeV was obtained in Ref. [25] by multiplying the SPP by the normalization factor of $\mathrm{N}_I = 0.25$. This value is significantly smaller than that ($N_I = 0.78$) obtained for many systems involving tightly bound nuclei [27].

It is worth mentioning that, for all energies, the CRC calculations were performed by using the same set of parameter values for the nuclear potential, deformation lengths, and spectroscopic factors. These values were determined in Ref. [25], through the analyses of the data for $E_{\mathrm{LAB}} = 37.5$ MeV. In this

sense, the data analyses for the other energies were performed here without adjustable parameters.

The CRC calculations provide a good overall description of the complete data set, except in the Fresnel angular region for the elastic scattering at 33.5 and 37.5 MeV. In fact, the data at 33.5 MeV present a pronounced Fresnel peak which is not reproduced by the theoretical calculations. On the other hand, according to our theoretical approaches, a Fresnel peak is expected at 37.5 MeV around 100°, but without correspondence in the experimental data. A similar result has been recently reported in Ref. [33] for the elastic scattering of ^{9}Be on ^{120}Sn. In this case, the Fresnel peak is prominent in the data at $E_{\rm LAB} = 29.5$ MeV, damped at $E_{\rm LAB} = 31$ MeV, and again appears in higher energies (42 and 50 MeV). This behavior is not foreseen by the CDCC theoretical calculations reported in that paper.

To investigate the effect of the couplings to the continuum on the elastic-scattering cross sections, we have also performed CDCC calculations considering the breakup of ^{10}B into ^{4}He plus ^{6}Li. However, according to our theoretical results, this effect is quite small and, therefore, the discrepancy commented above between theory and experiment in the Fresnel region is still not understood. The discrepancy at the specific energy of 33.5 MeV is not related to any kind of contamination or normalization issue, since no similar behavior is found in the data sets for the other energies. It would be of value to measure elastic scattering of ^{10}B from ^{120}Sn at higher energies, with the purpose of comparison with the behavior commented above for ^{9}Be + ^{120}Sn.

ACKNOWLEDGMENTS

This work has been partially supported by Fundação de Amparo à Pesquisa do Estado de São Paulo (FAPESP), Conselho Nacional de Desenvolvimento Científico e Tecnológico (CNPq), Coordenação de Aperfeiçoamento de Pessoal de Nível Superior (CAPES), and Fundação de Amparo à Pesquisa do Estado do Rio de Janeiro (FAPERJ), Brazil. This work is a part of the project INCT-FNA Proc. N° 464898/2014-5. This work has also been partially supported by the Spanish Ministerio de Economía y Competitividad, and the European Regional Development Fund (FEDER) under Project No. FIS2014-51941-P, by Junta de Andalucía under Group No. FQM-160, and by the European Union's Horizon 2020 research and innovation program under Grant Agreement No. 654002. M.A.G.A. would like to thank the VI Plan Propio de Investigación y Transferencia–Universidad de Sevilla (2017 and 2018).

[1] C. Charbonnel and F. Primas, Astronomy Astrophys. **442**, 961 (2005).
[2] I. Tanihata, H. Savajols, and R. Kanungo, Prog. Part. Nucl. Phys. **68**, 215 (2013).
[3] S. Gales, Prog. Part. Nucl. Phys. **59**, 22 (2007).
[4] T. Motobayashi, Prog. Part. Nucl. Phys. **59**, 32 (2007).
[5] A. Lèpine-Szily, R. Lichtenthaler, and V. Guimarães, Eur. Phys. J. A **50**, 128 (2014).
[6] C. Bertulani and A. Gade, Phys. Rep. **485**, 195 (2010).
[7] I. Tanihata, H. Hamagaki, O. Hashimoto, Y. Shida, N. Yoshikawa, K. Sugimoto, O. Yamakawa, T. Kobayashi, and N. Takahashi, Phys. Rev. Lett. **55**, 2676 (1985).
[8] M. Mazzocco *et al.*, Eur. Phys. J. A **28**, 295 (2006).
[9] D. Escrig *et al.*, Nucl. Phys. A **792**, 2 (2007).
[10] A. M. Sánchez-Benítez *et al.*, Nucl. Phys. A **803**, 30 (2008).
[11] L. Acosta *et al.*, Eur. Phys. J. A **42**, 461 (2009).
[12] L. Acosta, A. M. Sánchez-Benítez, M. E. Gómez, I. Martel, F. Peréz-Bernal, F. Pizarro, J. Rodríguez-Quintero, K. Rusek, M. A. G. Alvarez, M. V. Andrés, J. M. Espino, J. P. Fernández-García, J. Gómez-Camacho, A. M. Moro, C. Angulo, J. Cabrera, E. Casarejos, P. Demaret, M. J. G. Borge, D. Escrig, O. Tengblad, S. Cherubini, P. Figuera, M. Gulino, M. Freer, C. Metelko, V. Ziman, R. Raabe, I. Mukha, D. Smirnov, O. R. Kakuee, and J. Rahighi, Phys. Rev. C **84**, 044604 (2011).
[13] M. Cubero, J. P. Fernández-García, M. Rodríguez-Gallardo, L. Acosta, M. Alcorta, M. A. G. Alvarez, M. J. G. Borge, L. Buchmann, C. A. Diget, H. A. Falou, B. R. Fulton, H. O. U. Fynbo, D. Galaviz, J. Gómez-Camacho, R. Kanungo, J. A. Lay, M. Madurga, I. Martel, A. M. Moro, I. Mukha, T. Nilsson, A. M. Sánchez-Benítez, A. Shotter, O. Tengblad, and P. Walden, Phys. Rev. Lett. **109**, 262701 (2012).
[14] A. Di Pietro, G. Randisi, V. Scuderi, L. Acosta, F. Amorini, M. J. G. Borge, P. Figuera, M. Fisichella, L. M. Fraile, J. Gómez-Camacho, H. Jeppesen, M. Lattuada, I. Martel, M. Milin, A. Musumarra, M. Papa, M. G. Pellegriti, F. Perez-Bernal, R. Raabe, F. Rizzo, D. Santonocito, G. Scalia, O. Tengblad, D. Torresi, A. Maira Vidal, D. Voulot, F. Wenander, and M. Zadro, Phys. Rev. Lett. **105**, 022701 (2010).
[15] J. P. Fernández-García *et al.*, Phys. Rev. Lett. **110**, 142701 (2013).
[16] J. P. Fernández-García *et al.*, Phys. Rev. C **92**, 044608 (2015).
[17] R. Rafiei, R. du Rietz, D. H. Luong, D. J. Hinde, M. Dasgupta, M. Evers, and A. Diaz-Torres, Phys. Rev. C **81**, 024601 (2010).
[18] D. H. Luong *et al.*, Phys. Lett. B **695**, 105 (2011).
[19] S. Kalkal, E. C. Simpson, D. H. Luong, K. J. Cook, M. Dasgupta, D. J. Hinde, I. P. Carter, D. Y. Jeung, G. Mohanto, C. S. Palshetkar, E. Prasad, D. C. Rafferty, C. Simenel, K. Vo-Phuoc, E. Williams, L. R. Gasques, P. R. S. Gomes, and R. Linares, Phys. Rev. C **93**, 044605 (2016).
[20] J. P. Fernández-García, M. A. G. Alvarez, and L. C. Chamon, Phys. Rev. C **92**, 014604 (2015).
[21] D. F. M. Botero, L. C. Chamon, and B. V. Carlson, J. Phys. G **44**, 105102 (2017).
[22] W. J. Vermeer, R. K. Bhalla, and A. R. Poletti, Phys. Rev. C **28**, 432 (1983).
[23] L. C. Chamon and B. V. Carlson, Nucl. Phys. A **846**, 1 (2010).
[24] V. A. B. Zagatto, J. Lubian, L. R. Gasques, M. A. G. Alvarez, L. C. Chamon, J. R. B. Oliveira, J. A. Alcántara-Núñez, N. H. Medina, V. Scarduelli, A. Freitas, I. Padron, E. S. Rossi, Jr., and J. M. B. Shorto, Phys. Rev. C **95**, 064614 (2017).
[25] L. R. Gasques, A. S. Freitas, L. C. Chamon, J. R. B. Oliveira, N. H. Medina, V. Scarduelli, E. S. Rossi, Jr., M. A. G. Alvarez, V. A. B. Zagatto, J. Lubian, G. P. A. Nobre, I. Padron, and B. V. Carlson, Phys. Rev. C **97**, 034629 (2018).

[26] L. C. Chamon, B. V. Carlson, L. R. Gasques, D. Pereira, C. De Conti, M. A. G. Alvarez, M. S. Hussein, M. A. Cândido Ribeiro, E. S. Rossi, Jr., and C. P. Silva, Phys. Rev. C **66**, 014610 (2002).
[27] M. A. G. Alvarez *et al.*, Nucl. Phys. A **723**, 93 (2003).
[28] Y. Sakuragi, M. Yahiro, and M. Kamimura, Prog. Theor. Phys. Suppl. **89**, 136 (1986).
[29] G. H. Rawitscher, Phys. Rev. C **9**, 2210 (1974).
[30] G. H. Rawitscher, Nucl. Phys. A **241**, 365 (1975).
[31] M. Kamimura *et al.*, Prog. Theor. Phys. Suppl. **89**, 1 (1986).
[32] N. Austern *et al.*, Phys. Rep. **154**, 125 (1987).
[33] A. Arazi, J. Casal, M. Rodríguez-Gallardo, J. M. Arias, R. Lichtenthäler Filho, D. Abriola, O. A. Capurro, M. A. Cardona, P. F. F. Carnelli, E. de Barbará, J. Fernández Niello, J. M. Figueira, L. Fimiani, D. Hojman, G. V. Martí, D. Martínez Heimman, and A. J. Pacheco, Phys. Rev. C **97**, 044609 (2018).